Photochemical & Photobiological Sciences (2022) 21:1101–1109
https://doi.org/10.1007/s43630-022-00202-6

ORIGINAL PAPERS

Photodynamic disinfection of SARS-CoV-2 clinical samples using a methylene blue formulation

Catarina S. Lobo[1] · Paulo Rodrigues-Santos[2,3,4] · Dina Pereira[2] · Jisette Núñez[5,2] · João C. D. Trêpa[7] · David Lopes Sousa[7] · Jorge Vaz Lourenço[7] · Maria Filomena Coelho[7] · Luis Pereira de Almeida[5,2,6] · José Saraiva da Cunha[7] · Luis G. Arnaut[8]

Received: 22 December 2021 / Accepted: 2 March 2022 / Published online: 19 March 2022

Keywords Photodynamic inactivation · Photodisinfection · Antimicrobial photodynamic disinfection · Methylene blue · SARS-CoV-2 · Pseudotyped lentiviral vector

1 Introduction

Global awareness of the potentially devastating consequences of the COVID-19 pandemic favored an unprecedented concentration of efforts in science and medicine to find clinical solutions for thousands of new patients every day. The structure of the coronavirus transmembrane spike (S) glycoprotein, which promotes the entry of SARS-CoV-2 into cells, was readily determined [1]. The S glycoprotein comprises a S1 subunit that mediates binding to the host receptor and a S2 subunit that induces fusion of the viral envelope with cellular membranes. Cellular entry is promoted by tight binding between SARS-CoV-2 and the human angiotensin-converting enzyme 2 (hACE2), which also explains the efficient transmission of SARS-CoV-2 in humans. The entry receptor hACE2 and the viral entry-associated protease are highly expressed in nasal epithelial cells, which highlights their role in initial infection and also as possible reservoirs for dissemination within or between individuals [2]. These findings paved the way to the design of diagnostics, vaccines and therapeutics for COVID-19.

The S glycoprotein forms an extensive crown on the virus surface and is an appealing target for monoclonal antibody therapies. Bamlanivimab was the first monoclonal antibody approved by the FDA for COVID-19, in November 2020. However, its marketing authorization was revoked in April 2021 in view of the sustained increase of SARS-CoV-2 viral variants that were resistant to bamlanivimab alone, resulting in the increased risk for treatment failure. Meanwhile, the use of bamlanivimab and etesevimab administered together was approved by the FDA in February 2021, and the authorization for their administration together to mild-to-moderate COVID-19 patients was maintained. Another combination of monoclonal antibodies, casirivimab and imdevimab, had been approved in November 2020 for the same indication. May 2021, the FDA approved the monoclonal antibody sotrovimab which targets the S protein. Tocilizumab, a recombinant humanized monoclonal antibody that inhibits binding of interleukin-6 (IL-6) to both membrane and soluble IL-6 receptors, was approved June 2021 for mild-to-moderate patients receiving systemic corticoids and requiring supplemental oxygen.

The repositioning of existing drugs to treat COVID-19 has been less successful than the development of antibody therapies. In October 2020, the FDA approved remdesivir,

✉ Luis G. Arnaut
lgarnaut@qui.uc.pt

1 LaserLeap Technologies, R. Cel. Júlio Veiga Simão, CTCV, Ed. B, 3025-307 Coimbra, Portugal

2 Center for Neuroscience and Cell Biology (CNC), University of Coimbra, 3004-517 Coimbra, Portugal

3 Faculty of Medicine (FMUC), Institute of Immunology, University of Coimbra, Coimbra, Portugal

4 Center of Investigation in Environment, Genetics and Oncobiology (CIMAGO), Faculty of Medicine, University of Coimbra, Coimbra, Portugal

5 Faculty of Pharmacy, University of Coimbra, 3000-548 Coimbra, Portugal

6 ViraVector—Infrastructure of the National Roadmap for Production of Viral Vectors for Gene Transfer, Coimbra, Portugal

7 Centro Hospitalar e Universitário de Coimbra, Coimbra, Portugal

8 CQC, Chemistry Department, University of Coimbra, 3004-535 Coimbra, Portugal

a broad-spectrum antiviral, as the first treatment for COVID-19, based on three randomized trials, where it was shown that hospitalized patients recovered faster and had relief of symptoms relative to control groups. Although remdesivir is a milestone in the treatment of COVID-19, mortality and morbidity remained high. It was also recognized very early in the management of the pandemic that patients with severe COVID-19 have a cytokine storm syndrome, with increased IL-6 and other cytokine serum levels, which correlate with the severity of the disease [3]. It was suggested that patients with hyperinflammation could benefit from selective cytokine blockade and Janus kinase (JAK) inhibition [4]. In a remarkable tour-de-force of Artificial Intelligence, it was possible to identify baricitinib, approved for rheumatoid arthritis, as having potential antiviral and anticytokine activity [5]. Baricitinib is a JAK inhibitor that interferes with the pathway that leads to inflammation. The combination of baricitinib with remdesivir proved superior to remdesivir alone in COVID-19 patients receiving oxygen or non-invasive ventilation [6]. FDA approved this combination in November 2020, but NIH issued guidelines that recommend the use of this combination in patients receiving oxygen but not receiving corticosteroids. Previously, in June 2020, a press release disclosed that dexamethasone, a potent anti-inflammatory corticosteroid with broad effects on innate and adaptive immunity, could reduce by 8–26% the 28-day mortality of patients with severe COVID-19 [7]. Dexamethasone was adopted for the management of critically ill patients even before the actual publication of the clinical trial results, which showed a reduction of mortality relative to the usual care group of 29.3% vs 41.4% for patients with invasive ventilation, and of 23.3% vs 26.2% for patients receiving oxygen alone [8]. Currently, dexamethasone is recommended for use alone or in combination with remdesivir for patients who require supplemental oxygen. A variety of other small molecules showed efficacy in vitro against SARS-CoV-2 and were proposed for COVID-19 treatment, but did not yet translate to meaningful clinical benefits [9, 10]. A good example is methylene blue (MB), which exhibited a concentration-dependent inhibition of SARS-CoV-2 binding to hACE2 with $EC_{50} = 3.0$ µM according to some authors [11], or as low as 0.3 µM according to others [12]. These EC_{50} values are lower than those reported for remdesivir (23 µM) [13]. At this concentration level, an assay involving 48 h exposure showed that MB inhibited the entry of a pseudovirus bearing the SARS-CoV-2 S protein into hACE2-expressing HEK293T cells [11]. MB has been in clinical use in various antimicrobial fields for a century [14], and its use was approved by the FDA for the treatment of patients with acquired methemoglobinemia, opening the way for drug repurposing. MB is also one of the most widely used and better characterized photosensitizers, with remarkable clinical effect in a variety of infectious diseases [15]. Interestingly, a cohort of 2500 patients treated among others with MB for cancer care did not develop influenza-like illness during the COVID-19 pandemic, suggesting that MB played a protective role [16].

According to the COVID Data Tracker of the Centers for Disease Control and Prevention, 1 year of approved therapies and vaccination of > 50% of the US population did not manage to lower the lethality of COVID-19 below 1%. A COVID-19 therapy when the first symptoms are detected would be most welcome to manage this pandemic.

Photodynamic disinfection (PDI) was proposed as an alternative approach to inactivate SARS-CoV-2 [17–21], and clinical use of PDI in COVID-19 patients has been published [22, 23]. The advantage of PDI is that it uses photosensitizer molecules that do not have pharmacological effect unless they are electronically excited with light of an appropriate wavelength and in the presence of molecular oxygen. The electronically excited photosensitizer has the ability to transfer its excess energy, or an electron, to molecular oxygen and generate single oxygen, or superoxide ion. These species, and other reactive oxygen species (ROS) eventually formed, have short lifetimes and react with biomolecules in the illuminated volume [24]. The oxidative stress produced can inactivate microorganisms or, under appropriate doses and drug-to-light intervals, trigger cell death [25]. The obvious advantage of PDI is that it can target tissues with laser light: the pharmacological effect is restricted to the illuminated volume and systemic toxicity is avoided. It has been emphasized that PDI is a good candidate for treating COVID-19, because SARS-CoV-2 is an enveloped RNA virus and these viruses are most sensitive to PDI [26]. In addition, the use of light to treat airway related infections is relatively common. Among the various photosensitizers that have been used in PDI of microorganisms, MB has a special interest, because it is used for other diseases and may inhibit SARS-CoV-2 replication in the dark. The mechanism of virus inactivation with MB-PDI has been investigated in detail and shown to involve both oxidation of proteins and damage to RNA [27]. Photoinduced modification of RNA enables the use of real time PCR methods to determine amplification inhibition with MB-PDI [28]. The inactivation of SARS-CoV-2 with MB-PDI was recently explored by Loktev and coworkers [29]. Our work describes PDI of clinical samples collected from the surface of the respiratory mucosa of COVID-19 patients with nasopharyngeal swabs. We show that > 99.99% amplification inhibition can be obtained within 1 min laser illumination when an appropriate MB formulation is used. We also show that under these conditions MB-PDI has low toxicity to eukaryotic cells and inhibits the infection of human embryonic kidney cells overexpressing the hACE2 gene.

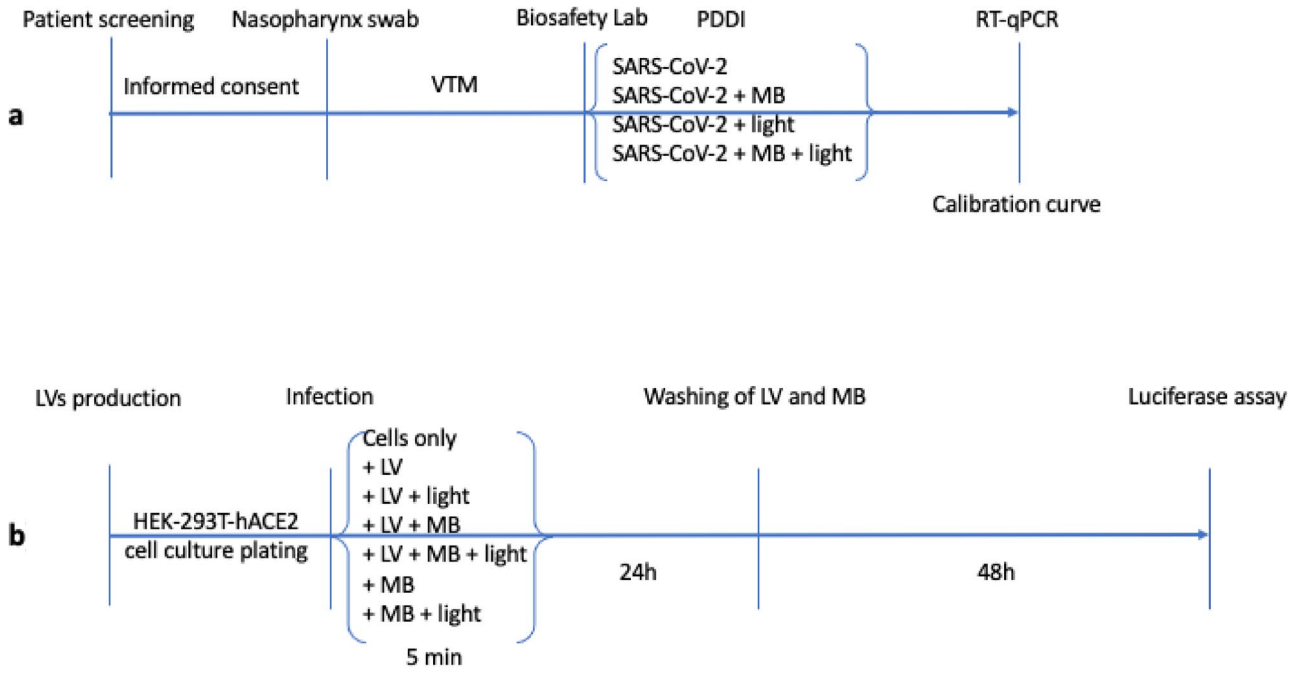

Fig. 1 Design of the PDI of virus. **a** SARS-CoV-2 in clinical samples. **b** SARS-CoV-2 pseudotyped lentiviral vectors (LVs) encoding for luciferase and exhibiting the S protein at the surface. *VTM* viral transport medium

2 Results and discussion

This interventional clinical study employed a diagnostic procedure currently used in COVID-19 disease to collect clinical samples of SARS-CoV-2 viruses. The study protocol was approved by the ethical committee of the University of Coimbra Hospital Center (CHUC). Informed consent was obtained from all participating patients, aged older than 18 years and hospitalized in CHUC, that volunteered for the study. The SARS-CoV-2 samples were taken from the participant's nasopharynx using a swab, immediately transferred to a viral transport medium (VTM) and transported within 3 h to a biosafety level-2 laboratory, where they were stored under refrigeration and analyzed.

The flow diagram of SARS-CoV-2 study is shown in Fig. 1a. The MB-based commercial formulation (0.01% w/v MB and 0.25% w/v chlorhexidine gluconate in an adjuvant aqueous base) and the illumination system (~860 mW at 670 nm, equally divided between two illuminators) employed in PDI of SARS-CoV-2 are similar to those previously employed in PDI of MRSA [30] and of *S. pyogenes* [31]. These earlier studies evaluated the feasibility of photoinactivating bacteria colonizing the nose of surgical patients, which are responsible for a large fraction of nosocomial infections. Based on the results of such studies, we selected a MB formulation dilution of 1:20 (MB-1:20) and 4 or 8 min of illumination to inactivate SARS-CoV-2 in the first set of clinical samples. This dilution corresponds to a MB concentration of 15 μM, but it is more appropriate to refer the dilution factor than the MB concentration because of the presence of adjuvants in the formulation. Each clinical sample was divided to obtain triplicates for each experimental condition and two RT-qPCR measurements were made and averaged for each triplicate. A calibration curve employing dilutions of a freshly prepared standard was employed to convert cycle threshold (Ct) values into viral loads (copies/mL).

Figure 2a shows that 4 min of illumination in the presence of MB-1:20 were sufficient to obtain a percentage amplification inhibition > 99.999%. Subsequent clinical samples were illuminated for 2 min or for 1 min. Figure 2b shows that 1 min illumination with a MB-1:20 reduced the virus titer in this sample below the detection limit of our setup. The highest Ct measured in this work was 43.89 (0.02 copies/mL, by extrapolation of the calibration curve). Based on the initial virus titer of this sample, the amplification inhibition is > 99.99%. Increasing the MB dilution to 100 (MB-1:100), with the same light dose, we found that a measurable quantity of virus remained in one of the samples after PDI (Fig. 2c), although this clinical sample had a relatively low virus titer. MB-1:100 and 25.8 J can be considered the lower limit to inactivate SARS-CoV-2 virus present in a 250 μL.

It is important to realize that the procedures to add SARS-CoV-2 and MB samples to the container, homogenize and illuminate with 25.8 J take less than 5 min. Hence, we evaluated the cytotoxicity and phototoxicity

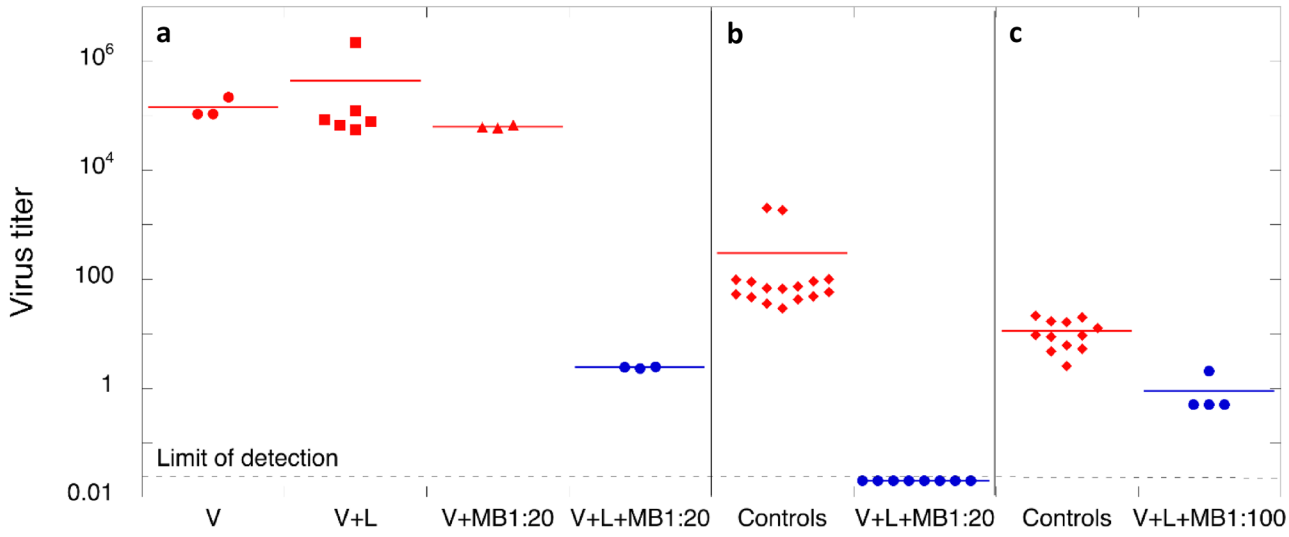

Fig. 2 PDI of three independent clinical samples. **a** MB-1:20 and 103.2 J (i.e., 4 min illumination); **b** MB-1:20 and 25.8 J (i.e., 1 min illumination); **c** MB-1:100 and 25.8 J (i.e., 1 min illumination). V = virus only; V + L = virus and light for 4 or 8 min; V + MB1:20 = virus and MB-1:20; V + L + MB1:20 = virus and light and MB-1:20; V + L + MB1:100 = virus and light and MB-1:100; Controls: virus alone or in the presence of MB without light, or in the presence of light but without MB

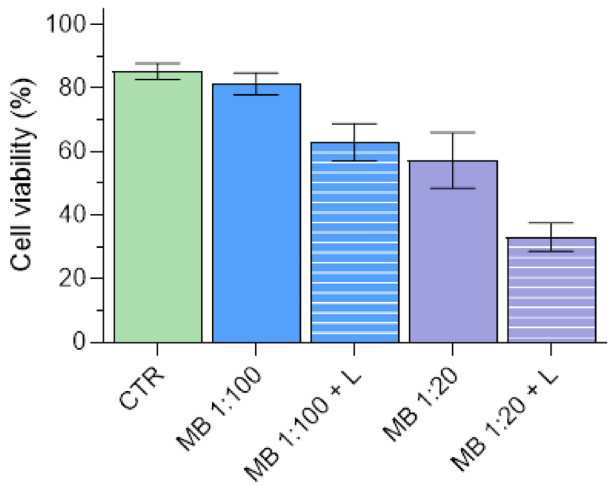

Fig. 3 Toxicity of the MB formulation towards HaCaT cells after 5 min of incubation, in the dark or exposed to 25.8 J at 670 nm. *CTR* untreated cells, *L* light

of the MB solutions towards human epidermal keratinocytes (HaCaT) cells with only 5 min of incubation. In the evaluation of phototoxicity, the 1 min of illumination is included in these 5 min of incubation. Figure 3 shows that cell viability in the presence of MB-1:100 but in the absence of light is indistinguishable from control and MB-1:20 is weakly cytotoxic under these conditions. MB-1:100 becomes weakly cytotoxic with exposure to 25.8 J at 670 nm. The illumination system employed for cells was the same as that employed for virus to allow a direct comparison between the two. Figure 3 also shows that the MB-1:20 becomes phototoxic with a light dose of 25.8 J.

Laser light at 670 nm alone or MB-1:20 alone for incubation times up to 8 min do not significantly damage the RNA of SARS-CoV-2. However, it is quite remarkable that MB-1:100 with 1 min illumination using 430 mW laser light produces a substantial reduction of the SARS-CoV-2 viral titer. This offers the opportunity to perform PDI of the nasal cavity and nasopharynx of COVID-19 patients with acceptable local phototoxicity and no systemic toxicity. This result is particularly interesting, because the evaluation of the photoinactivation is based on the viral RNA. The absence of viral RNA amenable to amplification in RT-qPCR after MB-PDI suggests that it was substantially damaged in just a few minutes. It is unlikely that, in less than 5 min, MB molecules penetrated virions, intercalated with viral nucleic acid and photo-inactivated it. The size of SARS-CoV-2 virions is ~ 100 nm [32] and the effective diffusion length of singlet oxygen is ~ 200 nm [15]. It is more likely that MB molecules adhered to viral envelope, generated singlet oxygen at the surface of the virions and the singlet oxygen diffused inside the particle, where it is more soluble than in the aqueous media, and then oxidized the viral RNA. It is well-known that singlet oxygen reacts with proteins, nucleotides and lipids with rate constants of ~ 10^4, ~ 10^3 and ~ 10^2 L/(g s), respectively [15]. This is a manifestation of the multi-target ability of ROS, often related to the fact that PDT is not readily associated with mechanisms of drug resistance. In particular, singlet oxygen reactions with guanosine are well-characterized and occur readily in photosensitization reactions [33]. These reactions are the most likely path to make

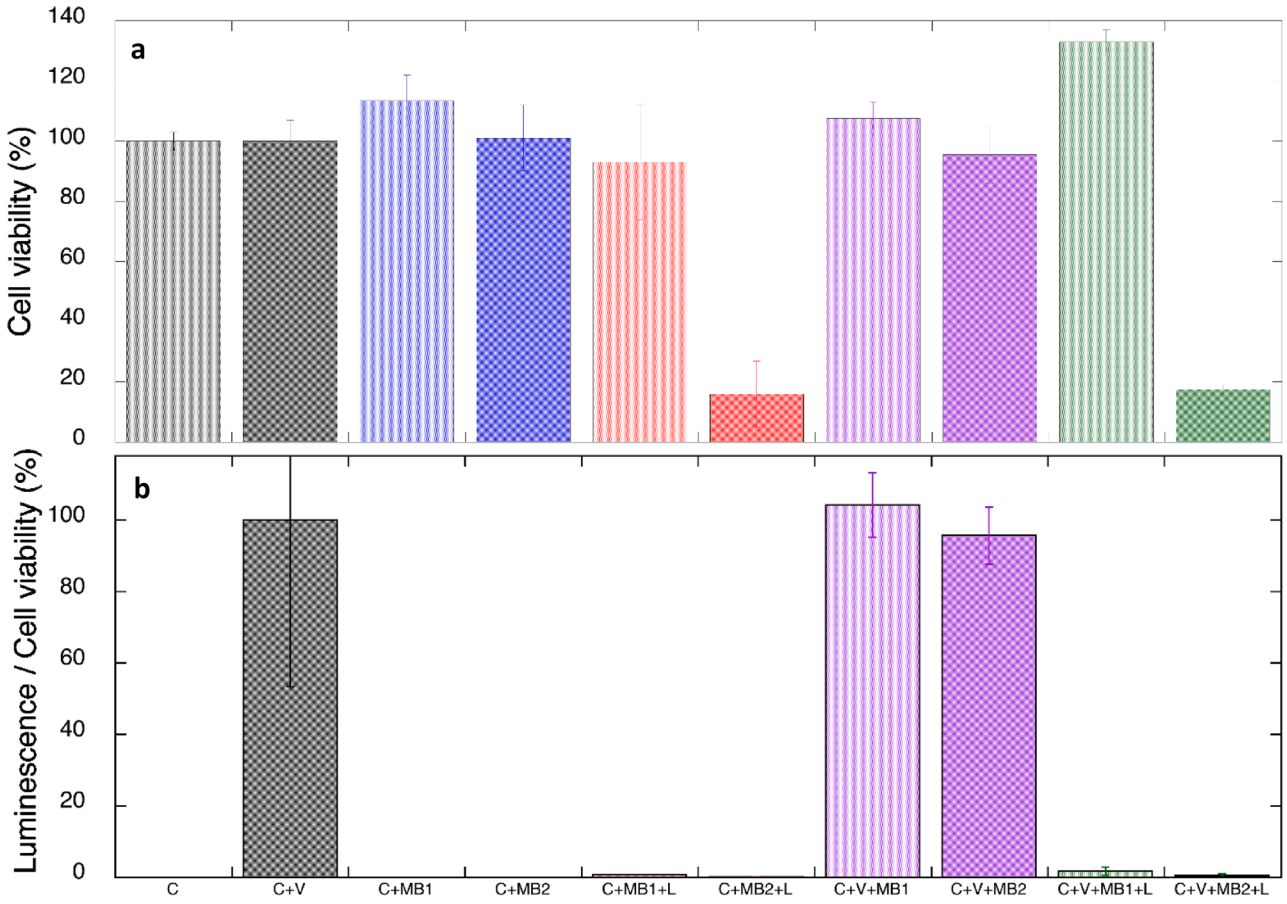

Fig. 4 Infection of HEK-293 T-hACE2 cells with SARS-CoV-2 pseudotyped lentivirus (LV). **a** Cell viability. **b** Ratio between chemiluminescence intensity and cell viability in %. C: cells with the addition of PBS; V: addition of LVs; MB1: [MB] = 3.2 μM; MB2: [MB] = 16 μM; L: light of 25 J

viral RNA undetectable by RT-qPCR. Earlier PDI studies with MB favored damage mechanisms involving MB intercalation with viral RNA but it is quite unexpected that this process could be efficiently completed in less than 5 min of incubation of MB.

To obtain a greater insight of how MB-PDI affects the ability of SARS-CoV-2 to infect cells, we also performed MB-PDI on SARS-CoV-2 pseudotyped lentiviral vectors (LVs), carrying S protein at its surface and encoding luciferase. Three major systems have been developed for viral vectors derived from HIV that differ in the number of plasmids used (2 to 4 plasmids) and aim at the minimization of viral gene recombination to reduce the possibility of reversion to the wild-type virus [34]. Here we employed a methodology using four major plasmids, two of them encoding for packaging genes, one for the envelope including S protein and the transfer gene, in this case the reporter gene luciferase. Pseudotyped lentiviral vectors (LVs) encoding luciferase were produced in HEK293T cells, as previously described [35], with slightly modifications, using polyethylenimine (PEI) [36]. We selected HEK-293 T-hACE2 cells for infection with our LVs, because these cells overexpress the hACE2 gene and SARS-CoV-2 infection is promoted by tight binding between the virion and hACE2. HEK-293 T-hACE2 cells are infected when they are incubated for 24 h with LVs. At this point the cells can be washed to remove the virion particles in the medium. Adding D-luciferin 72 h later, the chemiluminescence intensity of cultured cells reports on the extent of infection. Cells without the addition of LVs serve as positive controls of cell viability and negative controls of infection. Figure 1b illustrates the planning of this study.

We added various concentrations of the MB formulation to culture media with LVs and exposed the solutions to 1 min of laser light at 670 nm (25 J). The LVs and MB solutions were then added to HEK-293 T-hACE2 cells. Control experiments investigated cell viability and chemiluminescence when LVs were added to the cells alone, when added LVs and MB were not exposed to light, and when added LVs were exposed to light in the absence of MB. Figure 4 shows

that cell viability is not significantly affected in these cases and that chemiluminescence is observed when the luciferase assay is performed. As expected, the controls when LVs are not added to the cells give negative luciferase assays. We also investigated the cytotoxicity of the MB formulation for 24 h of incubation (see Supporting Information).

Successful MB-PDI should not compromise cell viability and should not give chemiluminescent cells. This is best evaluated in terms of the ratio between the chemiluminescence intensity and the cell viability to contemplate the trivial result of not observing chemiluminescence, because the cells died. Figure 4 shows experiments with two MB concentrations. At the highest concentration, [MB] = 16 μM, the illuminated MB formulation is cytotoxic, but it was only washed after 24 h of incubation. In a clinically relevant procedure, MB would be washed within 5 min of its application and low cytotoxicity is observed under such conditions (Fig. 3). In the case of the lower MB concentration, [MB] = 3.2 μM, and 1 min illumination no phototoxic products seem to have been generated, because cell viability is comparable to control, but the luciferase assay gave a chemiluminescence intensity 57 × lower per cell than in the case of LVs incubated alone with the HEK-293 T-hACE2 cells. This is sound evidence that MB-PDI can be used to inhibit the replication of SARS-CoV-2 under conditions of acceptable toxicity to human cells.

3 Conclusions

The mechanism of cellular entry by SARS-CoV-2 is through binding to angiotensin-converting enzyme 2 (ACE-2) and the pattern of ACE-2 expression provides evidence that the upper airway is the initial site of infection. In the early stages of SARS-CoV-2 infection, active virus infection and replication occurs in the apical layer of nasal and olfactory mucosa. Nasal photodisinfection with MB proved efficacious in the inactivation of multidrug-resistant bacteria colonizing the nose of surgical patients. Repurposing this procedure for the disinfection of the upper airways of COVID-19 patients immediately after the first positive diagnostic test may reduce the viral load, favoring recovering and reducing the spread of the disease. Our results show that MB-PDI of SARS-CoV-2 can achieve amplification inhibition > 99.99% at lower drug and light doses than currently employed for the photoinactivation of bacteria. Damage to viral RNA is achieved with incubation times shorter than 5 min. Inactivation of virus can be achieved with low micromolar MB concentrations and light doses (25.8 J) that are not toxic to human cells at such short incubation times. This offers the opportunity to provide safe, fast and efficient nasal photodisinfection of COVID-19 patients. A proof-of-concept clinical trial is presently exploring a nasal spray of MB formulation followed by 5 min of photoactivation using a nasal illuminator as a first line of defense against COVID-19 (ClinicalTrials.gov Identifier: NCT04615936).

4 Materials and methods

4.1 Reagents

The absorption spectrum of the MB formulation (Ondine NF-031 formulation, [MB] = 320 μM) at 1:100 dilution in water is presented in Figure S1. The band at 600 nm is characteristic of the presence of MB dimers in aqueous solutions [37]. Light at 670 nm will preferentially excite the monomer. The concentration of monomer will depend on dilution factors and, in clinical samples, on a variety of biomolecules and extraneous materials collected in the nasopharynx swabs. Using $\varepsilon_{664} = 10^5\ M^{-1}\ cm^{-1}$ for the monomer [38], we estimate that its concentration in the 1:100 diluted solution (MB-1:100) is ~ 2 μM. Our PDI studies employed 1:20 and 1:100 dilutions of the NF-031 formulation in water, which correspond to total MB concentrations of 16 μM and 3.2 μM, respectively.

4.2 Light source

The light source consisted of a two-channel fiber optic coupled CW laser source at 670 nm (Steriwave™ system and Nasal Light Illuminator Assembly, Ondine Biomedical Inc., Vancouver). The illuminator is coupled to the laser source to deliver the laser light in equal intensities through two optical fibers. To determine the output power of the nasal illuminator, a CW laser Omicron Laserage LDM750.1000. CWA.L.M, emitting at 749 nm, coupled with an optical fiber Medlight model FD was used as a reference. The light output power was measured using a Coherent LaserCheck detector, where all light of the reference laser was incident on the active area of the detector. The fiber was then inserted in the integrating sphere and the same detector placed in a proper location of the sphere to collect the scattered light. Using both measurements, a correction factor was determined correlating the light output power measured directly with the detector and through the integrating sphere. After determining this factor, by performing several measurements, the Nasal Light Illuminator was placed inside the sphere and the output power determined. The LaserCheck wavelength was set to the respective wavelengths to account for the differences of sensitivity. The laser output power measured with this method was 860 mW. The PDI studies employed light from only one of the fibers, i.e., a power of 430 mW.

4.3 Photodisinfection setup

Photodisinfection of SARS-CoV-2 and of lentivirus was performed in a plastic container injection-molded to conform to the shape of the illuminator, providing a close fit between the dispersion of laser light by the illuminator and the volume illuminated (Figure S2). The container was originally designed to simulate the conditions for nasal decolonization of asymptomatic MRSA surgical patients using PDI [30]. The same container was employed in the cell cytotoxicity and phototoxicity studies.

4.4 Clinical samples

We prepared a VTM containing Media Tech™ HBS solution with Ca^{2+} and Mg^{2+} but without Phenol Red (Corning, Manassas, VA, USA), with 2% sterile, heat-inactivated fetal bovine serum (FBS), 100 µg/mL gentamicin sulfate, 10,000 units/mL of penicillin, 10,000 µg/mL of streptomycin, and 25 µg/mL of Gibco Amphotericin B, to transport the clinical samples from the CHUC wards to a biosafety level-2 laboratory. Samples were initially collected from patients in intermediate care units, but the virus titer found was relatively small. Patients in these units typically had the first symptoms more than 5 days before the collection of the sample. It is known that the highest viral loads are detected in nasal swabs performed within the first week of the symptoms [39]. Hence, a second series of samples were collected from patients shortly after admission in emergency wards. A third series of samples was collected from patients admitted in any CHUC service that tested positive for COVID-19 upon admission and suspected to have a high viral load. Only the second and third series of samples, which had higher viral loads, were used for the quantification of SARS-CoV-2 before and after PDI.

4.5 Photoinactivation of clinical samples

An aliquot of 125 µL from the virus sample and another one from the appropriate solution (PBS or MB with the desired concentration), were placed in the container of Figure S2 to obtain a total volume of 250 µL. The nasal illuminator was fit in the container and the illumination was made for 1, 2, 4 or 8 min (25.8, 51.6, 103.2 or 206.4 J) in different clinical samples. Total RNA from control and treated samples was extracted with Roche High Pure Viral RNA kit, resuspended according to the manufacture instructions, and quantified by RT-qPCR.

4.6 Real-time reverse-transcription quantitative polymerase chain reaction (RT-qPCR)

RT-PCR provides real-time quantification of SARS-CoV-2 RNA in a sample by first reverse transcribing its RNA into DNA (RT step), and then amplifying the amount of nucleic acid (PCR step) for a certain number of cycles (Ct value) until the sample fluorescence exceeds a predefined threshold value. The cycle threshold (Ct) value is inversely related to the viral load and every ~ 3.3 increase in the Ct value reflects a tenfold reduction in starting material. We employed a Roche LightCycler 480 II System PCR platform and the genesig® Real Time PCR COVID-19 2G assay, a CE marked, in vitro diagnostic RT-PCR multiplex assay intended for the qualitative detection of nucleic acid from SARS-CoV-2 (ORF1ab and S gene targets) in nasopharyngeal swabs, oropharyngeal swabs and sputum specimens. The genesig® COVID-19 2G Primer & Probe Mix contains the primers and FAM labelled probe specific to the ORF1ab region of SARS-CoV-2 and the primers and Cy5 labeled probe specific to the S gene of SARS-CoV-2, as well as the primers and HEX labelled probe for the genesig RNA Internal extraction control (IEC). The concentration range used in the calibration curve was 2×10^2 to 3×10^6 copies/mL, which corresponded to a range of 30–16 cycles. The highest number of cycles measured for any sample was Ct = 43.89 (2.33×10^{-2} copies/mL, by extrapolation from the calibration curve). It is usual to consider a SARS-CoV-2 test positive when Ct < 40, and patients in the early stages of infection usually have Ct values of 20–30 or less [40]. A calibration curve was made for each one of the analysis of the samples with freshly prepared standards. Figure S3 presents a typical calibration curve. The results are presented in terms of the virus titer Q_t obtained from the calibration curve of the corresponding analysis. The virus titer can be very different from one patient to another. The percentage inhibition of amplification was calculated as $\left(1 - Q_t/Q_{ctr}\right) \times 100\%$, where Q_t and Q_{ctr} correspond to virus titer in treated and control samples.

4.7 Cytotoxicity towards human epidermal keratinocytes (HaCaT cells)

200.000 HaCaT cells were incubated with the various concentrations of the MB formulation for less than 5 min and illumination was performed with the 670 nm laser (25 J). After PDI, the samples were centrifuged to remove the MB and the pellet was resuspended in RPMI. Cell viability was assessed 24 h later by flow cytometry with the LIVE/DEAD™ Fixable Yellow Dead Cell Stain Kit (Fig. 2).

4.8 S-protein expressing lentivirus with reporter gene

Plasmids pRSV–Ver, pCMV-r8,92, and pRP[Exp]-CMV-human beta globin intron > {S (2020, deltaC19)-3xFLA (Vector Builder, Neu-Isenburg, Germany) were mixed with luciferase reporter transgene. HEK-293 T cells were

then transfected with a previously defined proportion of each plasmid [35], with slight modifications using polyethylenimine (PEI) at 1 mg/mL. After pseudoviral production and purification, quantification was performed using HIV-1 P24 Antigen ELISA kit from ZeptoMetrix. Pseudoviral validation was efficiently performed in previous studies (data not shown) by infecting HEK-293 T-hACE2 and HEK-293 T cells with the produced LVs at different dilutions for 72 h.

4.9 Infection of HEK-293 T-hACE2 cells

8.5×10^3 Human embryonic kidney cells permanently overexpressing the hACE2 gene (CoronaAssay-293 T cells (hACE2)–#: CACL-0012, Vector Builder), i.e., HEK-293 T-hACE2 cells, were plated in 96 multi-well plate with DMEM high glucose, without Phenol Red. Twenty-four hours later the cells were infected with previously photoinactivated or with control 60 ng/p24 pseudotyped lentiviral particles. PDI of the lentiviral particles was performed in the container of Figure S2 adding the MB formulation to the lentiviral particles in DMEM without phenol red, immediately followed by 1 min illumination with the Nasal Light Illuminator Assembly (25 J). The complete PDI procedure took less than 5 min. Media was replaced 24 h after infection and luminescence was analysed 72 h post-PDI using FLUOstar OMEGA (BMG Labtech GmbH) equipment and Luciferase Assay System Bright-Glo kit-Promega, according to manufacturer instructions. Cell viability was analysed by Alamar Blue assay with resazurin at 0.01 mg/mL prior to luciferase assay. Cell viability was also evaluated after 72 h of incubation of HEK-293 T-hACE2 cells with different concentrations of MB formulations using the procedure described above for HaCaT cells (Fig. S4).

Supplementary Information The online version contains supplementary material available at https://doi.org/10.1007/s43630-022-00202-6.

Acknowledgements The authors thank FCT and QREN/FEDER for funding (UIDB/QUI/00313/2020). LaserLeap acknowledges Centro2020 of PT2020 (European Regional Development Fund), for funding (Fotovid project nº 49708). We thank Ondine Biomedical (Canada) for access to a CE-marked Photodisinfection System.

Author contributions CSL performed the PDI studies. PRS made the RT-qPCR studies. DP and JG prepared and studied LVs. JCDT, DLS, JRL and MFC collected clinical samples. LPA conceived the LPs. JSC designed the clinical study. LGA conceived the studies and wrote the manuscript. All authors revised the manuscript.

Declarations

Conflict of interest On behalf of all authors, the corresponding author states that there is no conflict of interest.

References

1. Walls, A. C., Park, Y.-J., Tortorici, M. A., Wall, A., McGuire, A. T., & Veesler, D. (2020). Structure, function, and antigenicity of the sars-CoV-2 spike glycoprotein. *Cell, 181*, 281–292.
2. Sungnak, W., Huang, N., Bécavin, C., Berg, M., Queen, R., Litvinukova, M., Talavera-López, C., Maatz, H., Reichart, D., Sampaziotis, F., Worlock, K. B., Yoshida, M., Barnes, J. L., Banovich, N. E., Barbry, P., Brazma, A., Collin, J., Desai, T. J., Duong, T. E., Eickelberg, O., et al. (2020). SARS-CoV-2 entry factors are highly expressed in nasal epithelial cells together with innate immune genes. *Nature Medicine, 26*, 651–687.
3. Liu, F., Li, L., Xu, M., Wu, J., Luo, D., Zhu, Y., Li, B., Song, X., & Zhou, X. (2020). Prognostic value of interleukin-6, C-reactive protein, and procalcitonin in patients with COVID-19. *Journal of Clinical Virology, 127*, 104370.
4. Mehta, P., McAuley, D. F., Brown, M., Sanchez, E., Tattersall, R. S., & Manson, J. J. (2020). COVID-19: Consider cytokine storm syndromes and immunosuppression. *Lancet, 395*, 1033–1034.
5. Stebbing, J., Nievas, G. S., Falcone, M., Youhanna, S., Richardson, P., Ottaviani, S., Shen, J. X., Sommerauer, C., Tiseo, G., Ghiadoni, L., Virdis, A., Monzani, F., Rizos, L. R., Forfori, F., Céspedes, A. A., De Marco, S., Carrossi, L., Lena, F., Sánchez-Jurado, P. M., Lacerenza, L. G., et al. (2021). JAK inhibition reduces SARS-CoV-2 liver infectivity and modulates inflammatory responses to reduce morbidity and mortality. *Science Advances, 7*, eabe4724.
6. Kalil, A. C., Patterson, T. F., Mehta, A. K., Tomashek, K. M., Wolfe, C. R., Ghazaryan, V., Marconi, V. C., Ruiz-Palacios, G. M., Hsieh, L., Kline, S., Tapson, V., Iovine, N. M., & Members, A.-S.G. (2021). Baricitinib plus Remdesivir for Hospitalized Adults with Covid-19. *New England Journal of Medicine, 384*, 795–807.
7. RECOVERY trial. (2020). https://www.recoverytrial.net/results
8. The RECOVERY Collaborative Group (2021). Dexamethasone in hospitalized patients with covid-19. *New England Journal of Medicine, 384*, 693–704.
9. Wang, C., Wang, Z., Wang, G., Lau, J.Y.-N., Zhang, K., & Li, W. (2021). COVID-19 in early 2021: Current status and looking forward. *Sig. Transduct. Target. Ther., 6*, 114.
10. Jimenez-Aleman, G. H., Castro, V., Londaitsbehere, A., Gutierrez-Rodriguez, M., Garaigorta, U., Solano, R., & Gastaminza, P. (2021). SARS-CoV-2 fears green: the chlorophyll catabolite pheophorbide A is a potent antiviral. *Pharmaceuticals, 14*, 1048.
11. Bojadzic, D., Alcazar, O., & Buchwald, P. (2021). Methylene blue inhibits the SARS-CoV-2 spike–ACE2 protein-protein interaction–a mechanism that can contribute to its antiviral activity against COVID-19. *Frontiers in Pharmacology, 11*, 600372.
12. Gendrot, M., Andreani, J., Duflot, I., Boxberger, M., Le Bideau, M., Mosnier, J., Jardot, P., Fonta, I., Rolland, C., Bogreau, H., Hutter, S., La Scola, B., & Pradines, B. (2020). Methylene blue inhibits replication of SARS-CoV-2 in vitro. *International Journal of Antimicrobial Agent, 56*, 106202.
13. Choy, K. T., Wong, A. Y. L., Kaewpreedee, P., Sia, S. F., Chen, D. M., Hui, K. P. Y., Chu, D. K. W., Chan, M. C. W., Cheung, P.P.-H., Huang, X., Peiris, M., & Yen, H.-L. (2020). Remdesivir, Iopinavir, emetine, and homoharringtonine inhibit SARS-CoV-2 replication in vitro. *Antiviral Research, 178*, 104786.
14. Wainwright, M., & Crossley, K. B. (2013). Methyelene blue—a therapeutic dye for all seasons? *Journal of Chemotherapy, 14*, 431–443.
15. Aroso, R. T., Schaberle, F. A., Arnaut, L. G., & Pereira, M. M. (2021). Photodynamic disinfection and its role in controlling

infectious diseases. *Photochemical & Photobiological Sciences, 20*, 1497–1545.
16. Henry, M., Summa, M., Patrick, L., & Schwartz, L. (2020). A cohort of cancer patients with no reported cases of SARS-CoV-2 infection: The possible preventive role of methylene blue. *Substantia, 4*, 888.
17. Dias, L. D., & Bagnato, V. S. (2020). An update on clinical photodynamic therapy for fighting respiratory tract infections: a promising tool against COVID-19 and its co-infections. *Laser Physics Letters, 17*, 083001.
18. Dias, L. D., Blanco, K. C., & Bagnato, V. S. (2020). COVID-19: Beyond the virus. The use of photodynamic therapy for the treatment of infections in the respiratory tract. *Photodiagnosis and Photodynamic Therapy, 31*, 101804.
19. Almeida, A., Faustino, M. A. F., & Neves, M. G. P. M. S. (2020). Antimicrobial photodynamic therapy in the control of COVID-19. *Antibiotics, 9*, 320.
20. Sabino, C. P., Ball, A. R., Baptista, M. S., Dai, T., Hamblin, M. A., Ribeiro, M. S., Santos, A. L., Sellera, F. P., Tegos, G. P., & Wainwright, M. (2020). Light-based technologies for management of COVID-19 pandemic crisis. *Journal of Photochemistry and Photobiology B: Biology, 212*, 111999.
21. Kipshidze, N., Yeo, N., & Kipshidze, N. (2020). Photodynamic therapy for COVID-19. *Nature Photonics, 14*, 651–652.
22. Weber, H. B., Mehran, Y. Z., Orthaber, A., Saadat, H. H., Weber, R., & Wojcik, M. (2020). Successful reduction of SARS-CoV-2 viral load by photodynamic therapy (PDT) verified by QPCR—a novel approach in treating patients in early infection stages. *Medical Clinical Research, 5*, 311–325.
23. Schikora, D., Hepburn, J., & Plavin, S. R. (2020). Reduction of the viral load by non-invasive photodynamic therapy in early stages of COVID-19 infection. *American Journal Virology Disease, 2*, 01–05.
24. Dabrowski, J. M., & Arnaut, L. G. (2015). Photodynamic therapy (PDT) of cancer: From a local to a systemic treatment. *Photochemical & Photobiological Sciences, 14*, 1765–1780.
25. Donohoe, C., Senge, M. O., Arnaut, L. G., & Gomes-da-Silva, L. C. (2019). Cell death in photodynamic therapy: From oxidative stress to anti-tumor immunity. *Biochimica et Biophysica Acta (BBA)-Reviews on Cancer, 1872*, 188308.
26. Wiehe, A., O'Brien, J. M., & Senge, M. O. (2019). Trends and targets in antiviral phototherapy. *Photochemical & Photobiological Sciences, 18*, 2565–2612.
27. Schneider, J. E., Jr., Tabatabaie, T., Maidt, L., Smith, R. H., Nguyen, X., Pye, Q., & Floyd, R. A. (1998). Potential mechanisms of photodynamic inactivation of virys by methylene blue. I. RNA-protein crosslinks and other oxidative lesions in Qß bacteriophage. *Photochemistry and Photobiology, 67*, 350–357.
28. Zhang, B., Zheng, L., Huang, Y.-Y., Mo, Q., Wang, X., & Qian, K. (2011). Detection of nucleic acid lesions dirung photochemical inactivation of RNA viruses by treatment with methylene blue and light using real-time PCR. *Photochemistry and Photobiology, 87*, 365–369.
29. Svyatchenko, V. A., Nikolnov, S. D., Mayorov, A. P., Gelfond, M. L., & Loktev, V. B. (2020). Antiviral photodynamic therapy: Inactivation and inhibition of SARS-CoV-2 in vitro using methylene blue and Radachlorin. *Photodiagnosis and Photodynamic Therapy, 33*, 102112.
30. Street, C. N., Pedigo, L., Giggs, A., & Loebel, N. G. (2009). Antimicrobial photodynamic therapy for the decolonization of methicillin-resistant Staphylococcus aureus from the anterior nares. *Proceedings of SPIE, 7380*, 73803B.
31. Cross, J., Romo, C., Andersen, R., & Loebel, N. G. (2020). Antimicrobial photodynamic therapy for rapid eradication of S Pyogenes. *Journal of Antimicrobial Agents, 6*, 187.
32. Klein, S., Cortese, M., Winter, S. L., Wachsmuth-Melm, M., Neufeldt, C. J., Cerikan, B., Stanifer, M. L., Boulant, S., Bartenschlager, R., & Chlanda, P. (2020). SARS-CoV-2 structure and replication characterized by in situ cryo-electron tomography. *Nature Communications, 11*, 5885.
33. Ye, Y., Muller, J. G., Luo, W., Mayne, C. L., Shallop, A. J., Jones, R. A., & Burrows, C. J. (2003). Formation of 13C-, 15N-, and 18O-labeled guanidinohydantoin from guanosine oxidation with singlet oxygen. Implications for structure and mechanism. *Journal of the American Chemical Society, 125*, 13926–13927.
34. Li, Q., Liu, Q., Huang, W., Li, X., & Wang, Y. (2017). Current status on the development of pseudoviruses for enveloped viruses. *Reviews in Medical Virology, 28*, e1963.
35. de Almeida, L. P., Ross, C. A., Zala, D., Aebischer, P., & Deglon, N. (2002). Lentiviral-mediated delivery of mutant huntingtin in the striatum of rats induces a selective neuropathology modulated by polyglutamine repeat size, huntingtin expression levels, and protein length. *Journal of Neuroscience, 22*, 3473–3783.
36. Wang, Q., Zhang, Y., Wu, L., Niu, S., Song, C., Zhang, Z., Lu, G., Quiao, C., Hu, Y., Yuen, K. Y., Wang, Q., Zhou, H., Yan, J., & Qi, J. (2020). Structural and functional basis of SARS-CoV-2 entry by using human ACE2. *Cell, 181*, 898–904.
37. Nuñez, S. C., Yoshimura, T. M., Ribeiro, M. S., Junqueira, H. C., Maciel, C., Coutinho-Neto, M. D., & Baptista, M. S. (2015). Urea enhances the photodynamic efficiency of methylene blue. *Journal of Photochemistry and Photobiology, B: Biology, 150*, 31–37.
38. Fernández-Pérez, A., & Marbán, G. (2020). Visible light spectroscopic analysis of methylene blue in water; what comes after dimer? *ACS Omega, 5*, 29801–29815.
39. Zou, L., Ruan, F., Huang, M., Liang, L., Hauang, H., Hong, Z., Yu, J., Kang, M., Song, Y., Xia, J., Guo, Q., Song, T., He, J., Yen, H.-L., Peiris, P., & Wu, J. (2020). SARS-CoV-2 viral load in upper respiratory specimens of infected patients. *New England Journal of Medicine, 382*, 1177–1179.
40. Rhee, C., Kanjilal, S., Baker, M., & Klompas, M. (2020). Duration of severe acute respiratory syndrome coronavirus 2 (SARS-CoV-2) infectivity: When is it safe to discontinue isolation? *Clinical Infectious Diseases, 72*, 1467–1474.